Available online at www.sciencedirect.com
SCIENCE DIRECT®
Journal of Solid State Chemistry 177 (2004) 1746–1757
JOURNAL OF SOLID STATE CHEMISTRY
http://elsevier.com/locate/jssc

Phase relation studies in $Pb_{1-x}M'_xF_{2+x}$ systems ($0.0 \leqslant x \leqslant 1.0$; $M' = Nd^{3+}$, Eu^{3+} and Er^{3+})

A.K. Tyagi,* S.J. Patwe, S. N. Achary, and M.B. Mallia

Applied Chemistry Division, Bhabha Atomic Research Centre, Trombay, Mumbai 400 085, India

Received 26 July 2003; received in revised form 13 December 2003; accepted 30 December 2003

Abstract

In this communication we report the synthesis and characterization of a series of compounds with the general composition $Pb_{1-x}M'_xF_{2+x}$, ($0.0 \leqslant x \leqslant 1.0$; $M' = Nd^{3+}$, Eu^{3+} and Er^{3+}) to elucidate the detailed phase relations between PbF_2 and $M'F_3$. These three rare-earth fluorides were selected so as to delineate the effect of ionic size on the phase relations. In all the three systems, fluorite-type solid solutions are formed at the PbF_2 rich end. The solid solubility limits of NdF_3, EuF_3 and ErF_3 in the PbF_2 lattice, as observed from this study, are 30, 25 and 15 mol%, respectively. In PbF_2–NdF_3 system, beyond the fluorite-type solid solutions, NdF_3 phase is observed. However, in both PbF_2–EuF_3 and PbF_2–ErF_3 systems, certain fluorite related ordered phases, namely, a rhombohedral phase with about 40 mol% of EuF_3 or ErF_3 in PbF_2, and a tetragonal phase with 45–50 mol% of ErF_3 in PbF_2, are observed. In all the three systems, no solubility of the PbF_2 in the hexagonal or orthorhombic rare-earth fluoride lattice is observed. This is the first report on phase relation in these three systems under short annealed and slow cooled condition.

Keywords: Fluorides; X-ray diffraction; Phase equilibria

1. Introduction

The fluorite-type $PbF_2(\beta)$ and PbF_2 containing compounds have drawn a significant interest owing to their superionic properties [1]. The presence of frenkel anions in addition to a lone pair on Pb^{2+} makes them superior fluoride ion conductors compared to other fluorite-type fluorides, e.g., alkaline-earth fluorides [2]. Besides, the presence of lone pair, lower melting point of PbF_2 further facilitates the anion migration in the lattice. The ionic conductivity can be further enhanced by increasing the defects in the lattice. It was also reported that the ionic conduction of the PbF_2 could be significantly modified with non-stoichiometry created by aliovalent cation (viz. M'^{3+} ions) substitution in place of Pb^{2+} [3–6]. PbF_2 is highly prone to hydrolysis and also it has more affinity towards oxygen than fluorine. Thus, it is widely used as the deoxidizer in the growth of high purity crystals of various rare-earth fluorides and also to remove even the last traces of oxygen in the fluoride melt [7]. Due to its low melting and boiling points it can be removed easily leading to high purity crystals. Besides, PbF_2 and CdF_2 have been widely used in the preparation of transparent glass ceramic in lead-based glass systems, owing to the easier crystallization of the cubic PbF_2 or CdF_2 phases [8–10]. The segregation of rare-earth-doped ceramic phase in the transparent glass matrix poses interesting optical applications. The composition of the segregated phase in the glass matrix can be easily identified from the XRD data, if the XRD details of the corresponding pure crystalline phases are available on hand. Mortier et al. [9] have used such methods to identify the crystalline phases from the powder XRD data and based on that they explained their optical properties of glass ceramics. Therefore, it is important to investigate the crystalline phases in mixed fluoride systems from the point of view of characterization of optical transparent glass ceramics also. In order to know the maximum possible non-stoichiometric phases and the formation of various probable ordered phases, the phase relation in PbF_2–$M'F_3$ systems is used as an essential source of information. Thus, fluorite-type solid solutions in several of PbF_2–$M'F_3$ (M' = rare-earth ions) systems have been investigated under various experimental conditions [11–16]. However, to get the

*Corresponding author. Fax: +91-22-2550-5151/2511-9613.
E-mail address: aktyagi@magnum.barc.ernet.in (A.K. Tyagi).

0022-4596/$ - see front matter © 2004 Elsevier Inc. All rights reserved.
doi:10.1016/j.jssc.2003.12.036

reliable data on PbF_2-based systems, which are prone to hydrolysis, a short annealing condition needs to be optimized. Hence, it is worthwhile to investigate the existing and probable new phases with the rare-earth fluorides and PbF_2 under a short annealing condition. The detail results will also be useful in identifying the crystalline phase in partially crystallized lead-based fluoride or oxy-fluoride glass ceramics.

It is well known that the rare-earth fluorides crystallize in two different modifications, namely, hexagonal (tysonite) or orthorhombic (β-YF_3) structure depending on the ionic radii [17]. The lighter rare-earths fluorides (LaF_3 to PmF_3) have the hexagonal lattice whereas the heavier rare-earth fluorides (GdF_3 to LuF_3 including the YF_3) have the orthorhombic lattice. It is also reported that SmF_3 and EuF_3 exist in both types of structures depending upon the method of preparation. For the present study, the above-mentioned typical lattice types are represented by NdF_3, EuF_3 and ErF_3. This study is aimed at delineating the role of structure type of $M'F_3$ and ionic radii of the rare-earth ions on the phase width of the fluorite-type solid solutions and the ordering of the non-stoichiometric phases.

PbF_2 exists in orthorhombic (α) modification at room temperature and undergoes an irreversible phase transition to cubic-fluorite type structure [18]. Earlier, the unit cell details of some fluorite type solid solution compositions in PbF_2–ErF_3 system were reported in the context of identification of ceramic phase in ErF_3 containing $50GeO_2$–$40PbO$–$10PbF_2$ glasses [9]. A complete phase diagram in the PbF_2–YF_3 system had been given by Reau et al. [11]. They had reported the existence of three different types of phases, namely, fluorite-type solid solution, a rhombohedral phase similar to $A_4B_3F_{17}$ ($A = Sr^{2+}$, Ba^{2+}; $B = RE^{3+}$) as reported by Kaiser et al. [19], Sobolev and his coworkers [20]. Also, they reported a phase with composition $PbYF_5$ at lower temperatures. At higher temperatures they obtained a tysonite type phase at about 75 mol% of YF_3 and 25 mol% of PbF_2, which is stable only in a narrow temperature range. Subsequent study [12] on the phase relation on PbF_2–$M'F_3$ revealed that there are three different type phases, namely, fluorite-type solid solution, $A_4B_3F_{17}$ type phase and a tetragonal phase at composition of Pb_2YF_7. Sobolev and his coworkers had also published phase diagrams in PbF_2–$M'F_3$, M' = Lanthanides, Y and Sc [13–15]. However, in their studies they mentioned only about the fluorite-type solid solution and $A_4B_3F_{17}$ type phases. According to them the $A_4B_3F_{17}$ phase exists in a narrow composition range (± 1.5 mol% of $M'F_3$). They did not observe any tetragonal phase in their series. In a short annealed study of PbF_2–YF_3 system [16], it was found that the fluorite-type solid solution (up to 22 mol% of YF_3) and a rhombohedral $Pb_4Y_3F_{17}$ compound exist [21]. A pseudo-tetragonal phase was observed near the composition close to 50 mol% of YF_3 in PbF_2. In case of $M' = Sc^{3+}$, only cubic solid solution and after the saturation limit, separation of ScF_3 was observed. A comparison of earlier reported phase relations of MF_2–$M'F_3$ (M = Ca, Ba and Sr; M' = rare-earth ions) systems with the PbF_2–$M'F_3$ systems, indicate that although ionic radii of Pb^{2+} (1.29 Å) is very close to that of Sr^{2+} (1.26 Å), PbF_2 behaves differently from SrF_2, due to the lone pair on Pb^{2+}. The present study is carried out under short annealing and slow cooling condition and the results will supplement to the earlier reports on the phase relation in PbF_2 and $M'F_3$ systems.

2. Experimental

The starting materials NdF_3 and EuF_3 were synthesized by repeatedly heating Nd_2O_3 and Eu_2O_3 with excess of NH_4HF_2. The α-PbF_2 (Merck) and β-ErF_3 (Fluka) were dried before the use. Three series of nominal compositions with stoichiometry $Pb_{1-x}M'_xF_{2+x}$ ($0.00 \leqslant x \leqslant 1.00$ and $M' = Nd^{3+}$, Eu^{3+} and Er^{3+}) were prepared. About 300 mg of each mixture was pressed into a pellet of 6 mm diameter, wrapped in a platinum foil and sealed in an evacuated quartz tube. The tube was heated to 650°C at the rate of 4°C/min and held there for 4 h. The samples were cooled back to room temperature at a rate of 2°C/min. The powder XRD patterns of the products were recorded on a Philips (PW1710 model) X-ray diffractometer with Ni-filtered Cu-$K\alpha$ radiation. The detailed phase analyses of the three systems are explained in the following section.

3. Results and discussion

It was mentioned in the introduction that the metastable orthorhombic modification of PbF_2 transforms irreversibly to the cubic fluorite form at about 350°C. Thus, at the preparation temperature adopted in the present study, the orthorhombic structure of PbF_2 transformed to the cubic structure. From the XRD data of the nominal composition $Pb_{1-x}M'_xF_{2+x}$ (for $x = 1.0$), it was observed that NdF_3 has retained the hexagonal tysonite-type lattice and EuF_3 and ErF_3 have retained the orthorhombic lattice after the heat treatment. The low melting and superionic nature of the cubic PbF_2 makes the reaction fast enough to go for completion in a short time compared to alkaline-earth fluorides.

The further nominal compositions in the series $Pb_{1-x}M'_xF_{2+x}$ ($0.00 \leqslant x \leqslant 1.00$; $M' = Nd^{3+}$, Eu^{3+} and Er^{3+}) are characterized by comparing the successive XRD patterns of the respective series. The unit cell parameters of various phases are determined by indexing the observed reflections. Various phases identified in

these three systems are presented in Tables 1–3. The systematic phase analyses of various nominal compositions prepared in three systems of PbF_2–$M'F_3$ ($M' = Nd^{3+}$, Eu^{3+} and Er^{3+}) are summarized in Table 4. The PbF_2–$M'F_3$ systems can be grouped into three phase-regions, namely, a fluorite-type solid solution, fluorite related ordered phases and the rare-earth fluorides.

A comparison of the XRD patterns of the compositions $Pb_{1.00}M'_{0.00}F_{2.00}$ ($M' = Nd^{3+}$, Eu^{3+} and Er^{3+}) with those of the successive compositions in the respective series revealed their close similarity, indicating the solid solution formation up to a certain extent. However, the peak positions shift towards the higher angle side as the $M'F_3$ contents in the compositions increases, implying the contraction of the lattice. The solid solution formation was observed up to the nominal compositions $Pb_{0.70}Nd_{0.30}F_{2.30}$, $Pb_{0.75}Eu_{0.25}F_{2.25}$ and $Pb_{0.85}Er_{0.15}F_{2.15}$ in the respective series. The typical XRD patterns for the respective solid solution limits are shown in Fig. 1.

The solid solution of the fluorite-type lattice is the most common observation in the MF_2–$M'F_3$ (M = alkaline-earth cation and M' = rare-earth cation) systems [22]. These solid solutions have been explained with the anion-excess fluorite lattice [23,24]. The Pb^{2+} and the rare-earth ions are expected to be statistically distributed over the 4*a* site of the space group *Fm*3*m*. The excess-anions occupy the interstitial sites available in the fluorite lattice, namely, 32*f* ($x\,x\,x$, for $x = 0.40$) and 48*i* ($1/2\,x\,x$, for $0.35 \leqslant x \leqslant 0.40$) sites [23]. In the solid solution formation the inter-anionic repulsion can also displace some of the regular lattice site (8*c*) anions to these interstitial sites. Thus anions are distributed in the 8*c*, 48*i* and 32*f* sites forming a 222-type cluster. It can be emphasized here that even in the fluorite-type solid solution region the short-range anion clusters should not be ignored. Several reports dealing with the structural analyses show the presence of 222 type clusters in lower concentration of the $M'F_3$, whereas the presence of 432, 443 type clusters in the regions with higher concentration of the $M'F_3$ [23–26].

Table 1
Nominal compositions and their phase relations in $Pb_{1-x}Nd_xF_{2+x}$

S. No.	Nominal composition	mol% of NdF_3	Phase(s) present	a (Å)	b (Å)	c (Å)	V (Å)^3
1	$Pb_{1.00}Nd_{0.00}F_{2.00}$	0	C	5.942(1)	5.942(1)	5.942(1)	209.81(4)
2	$Pb_{0.95}Nd_{0.05}F_{2.05}$	5	C	5.937(0)	5.937(0)	5.937(0)	209.23(3)
3	$Pb_{0.90}Nd_{0.10}F_{2.10}$	10	C	5.927(0)	5.927(0)	5.927(0)	208.21(2)
4	$Pb_{0.85}Nd_{0.15}F_{2.15}$	15	C	5.921(0)	5.921(0)	5.921(0)	207.58(2)
5	$Pb_{0.80}Nd_{0.20}F_{2.20}$	20	C	5.917(1)	5.917(1)	5.917(1)	207.16(1)
6	$Pb_{0.75}Nd_{0.25}F_{2.25}$	25	C	5.905(0)	5.905(0)	5.905(0)	205.90(3)
7	$Pb_{0.70}Nd_{0.30}F_{2.30}$	30	C	5.895(1)	5.895(1)	5.895(1)	204.87(6)
8	$Pb_{0.65}Nd_{0.35}F_{2.35}$	35	C	5.895(0)	5.895(0)	5.895(0)	204.87(2)
			H	[a]			
9	$Pb_{0.60}Nd_{0.40}F_{2.40}$	40	C	5.895(1)	5.895(1)	5.895(1)	204.86(7)
			H	7.039(5)	7.039(5)	7.218(6)	309.7(4)
10	$Pb_{0.55}Nd_{0.45}F_{2.45}$	45	C	5.892(0)	5.892(0)	5.892(0)	204.50(2)
			H	7.033(4)	7.033(4)	7.187(5)	307.9(3)
11	$Pb_{0.50}Nd_{0.50}F_{2.50}$	50	C	5.890(0)	5.890(0)	5.890(0)	204.32(3)
			H	7.034(2)	7.034(2)	7.195(4)	308.3(2)
12	$Pb_{0.45}Nd_{0.55}F_{2.55}$	55	C	5.892(1)	5.892(1)	5.892(1)	204.60(3)
			H	7.038(2)	7.038(2)	7.209(4)	309.2(2)
13	$Pb_{0.40}Nd_{0.60}F_{2.60}$	60	C	5.892(0)	5.892(0)	5.892(0)	204.49(3)
			H	7.038(2)	7.038(2)	7.199(2)	308.8(2)
14	$Pb_{0.35}Nd_{0.65}F_{2.65}$	65	C	5.895(1)	5.895(1)	5.895(1)	204.87(7)
			H	7.037(2)	7.037(2)	7.198(2)	308.7(1)
15	$Pb_{0.30}Nd_{0.70}F_{2.70}$	70	C	5.895(2)	5.895(2)	5.895(2)	204.84(10)
			H	7.037(3)	7.037(3)	7.207(3)	309.1(2)
17	$Pb_{0.25}Nd_{0.75}F_{2.75}$	75	C	5.893(6)	5.893(6)	5.893(6)	204.7(3)
			H	7.035(1)	7.035(1)	7.198(2)	308.5(1)
19	$Pb_{0.20}Nd_{0.80}F_{2.80}$	80	C	5.888(6)	5.888(6)	5.888(6)	204.2(4)
			H	7.027(2)	7.027(2)	7.196(3)	307.8(2)
21	$Pb_{0.15}Nd_{0.85}F_{2.85}$	85	C	5.896(6)	5.896(6)	5.896(6)	205.0(4)
			H	7.033(1)	7.033(1)	7.204(1)	308.6(1)
24	$Pb_{0.10}Nd_{0.90}F_{2.90}$	90	C	5.90(1)	5.90(1)	5.90(1)	205.3(6)
			H	7.040(2)	7.040(2)	7.208(2)	309.4(2)
25	$Pb_{0.05}Nd_{0.95}F_{2.95}$	95	C	[a]			
			H	7.033(1)	7.033(1)	7.198(1)	308.33(8)
25	$Pb_{0.00}Nd_{1.00}F_{3.00}$	100	H	7.028(1)	7.028(1)	7.196(1)	307.8(1)

C = Cubic (fluorite) type, H = NdF_3 (hexagonal tysonite-type).
[a] Corresponding phases were not refined due to very insignificant intensities of reflections

Table 2
Nominal compositions and their phase relations in $Pb_{1-x}Eu_xF_{2+x}$

S. No.	Nominal composition	mol% of EuF_3	Phase(s) present	a (Å)	b (Å)	c (Å)	V (Å)^3
1	$Pb_{1.00}Eu_{0.00}F_{2.00}$	0	C	5.939(1)	5.939(1)	5.939(1)	209.51(3)
2	$Pb_{0.95}Eu_{0.05}F_{2.05}$	5	C	5.928(1)	5.928(1)	5.928(1)	208.28(4)
3	$Pb_{0.90}Eu_{0.10}F_{2.10}$	10	C	5.920(1)	5.920(1)	5.920(1)	207.48(8)
4	$Pb_{0.85}Eu_{0.15}F_{2.15}$	15	C	5.903(0)	5.903(0)	5.903(0)	205.66(2)
5	$Pb_{0.80}Eu_{0.20}F_{2.20}$	20	C	5.890(1)	5.890(1)	5.890(1)	204.29(3)
6	$Pb_{0.75}Eu_{0.25}F_{2.25}$	25	C	5.881(2)	5.881(2)	5.881(2)	203.4(1)
7	$Pb_{0.70}Eu_{0.30}F_{2.30}$	30	C	5.875(1)	5.875(1)	5.875(1)	202.75(6)
			R	[a]			
8	$Pb_{0.65}Eu_{0.35}F_{2.35}$	35	C	[a]			[a]
			R	4.134(1)	4.134(1)	10.126(1)	149.84(3)
9	$Pb_{0.60}Eu_{0.40}F_{2.40}$	40	R	4.132(1)	4.132(1)	10.119(1)	149.62(3)
				#4.125(1)	60.17(1)		49.84(2)
10	$Pb_{0.55}Eu_{0.45}F_{2.45}$	45	R	4.129(1)	4.129(1)	10.120(2)	149.62(3)
			O	[a]			
11	$Pb_{0.50}Eu_{0.50}F_{2.50}$	50	R	4.127(1)	4.127(1)	10.114(1)	149.19(4)
			O	6.611(5)	7.034(5)	4.390(3)	204.2(2)
12	$Pb_{0.45}Eu_{0.55}F_{2.55}$	55	R	4.127(1)	4.127(1)	10.111(1)	149.14(3)
			O	6.618(3)	7.027(3)	4.391(2)	204.2(2)
13	$Pb_{0.40}Eu_{0.60}F_{2.60}$	60	R	4.130(1)	4.130(1)	10.119(3)	149.48(7)
			O	6.621(3)	7.029(3)	4.396(2)	204.6(2)
14	$Pb_{0.35}Eu_{0.65}F_{2.65}$	65	R	4.129(1)	4.129(1)	10.117(2)	149.39(9)
			O	6.615(3)	7.025(3)	4.391(2)	204.1(2)
15	$Pb_{0.30}Eu_{0.70}F_{2.70}$	70	R	4.130(1)	4.130(1)	10.118(3)	149.49(7)
			O	6.619(3)	7.026(3)	4.391(2)	204.2(2)
17	$Pb_{0.25}Eu_{0.75}F_{2.75}$	75	R	4.135(2)	4.135(2)	10.121(6)	149.90(15)
			O	6.622(2)	7.031(3)	4.396(2)	204.7(1)
19	$Pb_{0.20}Eu_{0.80}F_{2.80}$	80	R	4.134(1)	4.134(1)	10.125(2)	149.86(6)
			O	6.622(4)	7.032(3)	4.398(2)	204.8(1)
21	$Pb_{0.15}Eu_{0.85}F_{2.85}$	85	R	4.130(1)	4.130(1)	10.113(2)	149.42(6)
			O	6.618(2)	7.028(3)	4.393(2)	204.3(1)
24	$Pb_{0.10}Eu_{0.90}F_{2.90}$	90	R	4.127(2)	4.127(2)	10.139(5)	149.55(14)
			O	6.620(1)	7.015(2)	4.394(1)	204.1(1)
25	$Pb_{0.05}Eu_{0.95}F_{2.95}$	95	R	[a]			
			O	6.623(1)	7.019(2)	4.397(1)	204.4(1)
25	$Pb_{0.00}Eu_{1.00}F_{3.00}$	100	O	6.626(1)	7.024(1)	4.401(1)	204.8(1)

C = Cubic (fluorite) type, R = Rhombohedral (Hexagonal settings), # = Rhombohedral (Rhombohedral settings), O = EuF_3 (orthorhombic YF_3-type).
[a] Corresponding phases were not refined due to very insignificant intensities of reflections or highly overlapping reflections.

The unit cell parameters of the saturated fluorite type solid solution limits are, 5.895(2) Å (for $Pb_{0.70}Nd_{0.30}F_{2.30}$), 5.881(2) Å (for $Pb_{0.75}Eu_{0.25}F_{2.25}$) and 5.874(2) Å (for $Pb_{0.85}Er_{0.15}F_{2.15}$) as against that of 5.942(2) Å for PbF_2. A typical plot of variation of unit cell parameter of the fluorite-type solid solution with composition indicating the lattice contraction is shown in Fig. 2. In the solid solution formation of MF_2–$M'F_3$, two significant but opposite factors, namely average cation radius and the inter-anionic repulsions, govern the unit cell dimension. Since the radii of the rare-earth ions in eight-fold coordination (ionic radii: Nd^{3+} = 1.11, Eu^{3+} = 1.07 and Er^{3+} = 1.00 Å) is quite smaller to Pb^{2+} ion (radius 1.29 Å), the average ionic radius of the metal ion sites usually decreases. However, the unit cell of the solid solution lattice contains excess of the fluoride ions, which tend to dilate the unit cell due to electrostatic repulsion. The overall effect of these two opposite factors decides the dilation or contraction of the lattice. In the earlier study of the PbF_2–YF_3 system the lattice contraction was observed in the solid solution region [16]. The solid solution formation in BaF_2–$M'F_3$ [21,24–26] always causes the lattice contraction whereas that of the CaF_2–$M'F_3$ ($M' = Y^{3+}$ and Nd^{3+}) system always causes lattice expansion [27,30]. In the present study, all the three systems show the lattice contraction, which implies that the decrease in the average cation radius dominates over the expansion caused by the inter-anion repulsion.

In the present study the typical solid solubility limit of NdF_3, EuF_3 and ErF_3 in PbF_2 is found to be 30, 25 and 15-mol%, respectively. In PbF_2–YF_3 system, Reau et al. [11] have observed 39 mol% as the solid solubility limit in the cubic PbF_2 at about 885°C, which decreases to about 13-mol% at 550°C. From the interpolation of these values, the expected solubility limit of YF_3 in PbF_2 should be about 22-mol% at 650°C. In the study of PbF_2–YF_3 system (annealed at 700°C for 3 h) shows a

Table 3
Nominal compositions and their phase relations in $Pb_{1-x}Er_xF_{2+x}$

S. No.	Nominal composition	mol% of ErF_3	Phase(s) present	a (Å)	b (Å)	c (Å)	V (Å)^3
1	$Pb_{1.00}Er_{0.00}F_{2.00}$	0	C	5.943(1)	5.943(1)	5.943(1)	209.90(4)
2	$Pb_{0.95}Er_{0.05}F_{2.05}$	5	C	5.916(1)	5.916(1)	5.916(1)	207.06(7)
3	$Pb_{0.90}Er_{0.10}F_{2.10}$	10	C	5.900(0)	5.900(0)	5.900(0)	205.34(2)
4	$Pb_{0.85}Er_{0.15}F_{2.15}$	15	C	5.874(2)	5.874(2)	5.874(2)	202.71(9)
5	$Pb_{0.80}Er_{0.20}F_{2.20}$	20	C	5.864(1)	5.864(1)	5.864(1)	201.65(4)
			R	[a]	[a]	[a]	
6	$Pb_{0.75}Er_{0.25}F_{2.25}$	25	C	5.874(1)	5.874(1)	5.874(1)	202.68(3)
			R	4.076(1)	4.076(1)	10.003(4)	143.95(8)
7	$Pb_{0.70}Er_{0.30}F_{2.30}$	30	C	5.878(1)	5.878(1)	5.878(1)	203.06(6)
			R	4.075(1)	4.075(1)	9.998(4)	143.79(9)
8	$Pb_{0.65}Er_{0.35}F_{2.35}$	35	C	5.878(1)	5.878(1)	5.878(1)	203.06(5)
			R	4.083(1)	4.083(1)	10.013(3)	144.53(8)
9	$Pb_{0.60}Er_{0.40}F_{2.40}$	40	R	4.078(1)	4.078(1)	10.006(2)	144.12(7)
				4.086(1)[#]	59.87(2)		48.08(3)
10	$Pb_{0.55}Er_{0.45}F_{2.45}$	45	T	4.064(1)	4.064(1)	5.811(2)	96.00(4)
11	$Pb_{0.50}Er_{0.50}F_{2.50}$	50	T	4.046(1)	4.046(1)	5.796(2)	94.86(5)
			O	[a]			
12	$Pb_{0.45}Er_{0.55}F_{2.55}$	55	T	4.050(1)	4.050(1)	5.803(2)	95.19(5)
			O	[a]			
13	$Pb_{0.40}Er_{0.60}F_{2.60}$	60	T	4.051(1)	4.051(1)	5.802(2)	95.21(6)
			O	6.343(4)	6.846(6)	4.397(3)	190.9(2)
14	$Pb_{0.35}Er_{0.65}F_{2.65}$	65	T	4.050(1)	4.050(1)	5.809(2)	95.29(4)
			O	6.335(3)	6.845(5)	4.406(3)	191.2(2)
15	$Pb_{0.30}Er_{0.70}F_{2.70}$	70	T	4.046(1)	4.046(1)	5.796(1)	94.89(3)
			O	6.342(3)	6.840(4)	4.382(3)	190.1(2)
17	$Pb_{0.25}Er_{0.75}F_{2.75}$	75	T	4.046(2)	4.046(2)	5.824(3)	95.35(8)
			O	6.332(5)	6.842(7)	4.397(4)	190.5(3)
19	$Pb_{0.20}Er_{0.80}F_{2.80}$	80	T	4.037(3)	4.037(3)	5.836(4)	95.1(1)
			O	6.333(2)	6.832(3)	4.383(2)	189.6(1)
21	$Pb_{0.15}Er_{0.85}F_{2.85}$	85	T	4.043(5)	4.043(5)	5.82(2)	95.1(4)
			O	6.343(1)	6.840(1)	4.381(1)	190.1(0)
24	$Pb_{0.10}Er_{0.90}F_{2.90}$	90	T	4.091(6)	4.091(6)	5.81(2)	94.9(4)
			O	6.341(1)	6.837(2)	4.381(1)	190.0(1)
25	$Pb_{0.05}Er_{0.95}F_{2.95}$	95	T	[a]			
			O	6.353(2)	6.853(3)	4.394(2)	191.3(1)
25	$Pb_{0.00}Er_{1.00}F_{3.00}$	100	O	6.354(1)	6.855(2)	4.395(1)	191.4(1)

C = Cubic (fluorite) type, R = Rhombohedral (Hexagonal setting) [#] = Rhombohedral (Rhombohedral settings), T = Tetragonal, O = ErF_3 (orthorhombic YF_3-type).

[a] Corresponding phases were not refined due to very insignificant intensities of reflections.

solubility limit of about 22-mol% of YF_3 [16]. Due to the similarity in the ionic radii of Er^{3+} and Y^{3+}, it is expected that ErF_3 should have similar solid solubility limit. The present observed solubility limit of ErF_3 in PbF_2 is still lower than the values reported for PbF_2–YF_3 system [11]. Dib et al. [12] concluded the solid solubility limit of YF_3 is about 17-mol% in spite of long annealed sample at 400–600°C. The authors also reported the solubility limit to be about 29-mol% at 800°C. The present observed value agrees with the corresponding values reported earlier [12] for YF_3. The solid solution behavior of the present study is closely similar to that reported for polycrystalline phase prepared by Mortier et al. [9] by slowly cooling the melt of the PbF_2–ErF_3 compositions. However, the higher solubility of ErF_3 in PbF_2 in glass matrix is due to the partial oxygen incorporation from the oxy-fluoride environment. The solid solubility limit of NdF_3 in PbF_2 lattice (30 mol%) is more close to that in BaF_2 (~35 mol%) [29], but, it is lower than that in SrF_2 (40 mol%) and CaF_2 (45 mol%) lattices [30]. Similarly, the observed solubility limit of EuF_3 in PbF_2 is also close to that in BaF_2 lattice [24]. The lower solubility values in the present case compared to that of BaF_2–$M'F_3$ ($M' = Nd^{3+}$, Eu^{3+} and Er^{3+}) systems [24,28,29], might be due to the low annealing temperature and shorter annealing time in the case of present investigation involving PbF_2.

The XRD patterns of the nominal compositions $Pb_{0.70}Eu_{0.30}F_{2.30}$ and $Pb_{0.65}Eu_{0.35}F_{2.35}$ appear similar to typical fluorite-type phases, however, the presence of some weak reflections at $2\theta \sim 25°$, 34°, 36°, 38°, 40° indicates either some sort of ordering in the fluorite-type lattice or appearance of some other phase. Besides, the

Table 4
Summary of the various phases identified in the PbF_2–$M'F_3$ ($M' = Nd^{3+}$, Eu^{3+} and Er^{3+} systems)

S. No.	Nominal composition	mol% of $M'F_3$	Phases identified		
			$M'F_3 = NdF_3$	EuF_3	ErF_3
1	$Pb_{1.00}M'_{0.00}F_{2.00}$	0	F	F	F
2	$Pb_{0.95}M'_{0.05}F_{2.05}$	5	F	F	F
3	$Pb_{0.90}M'_{0.10}F_{2.10}$	10	F	F	F
4	$Pb_{0.85}M'_{0.15}F_{2.15}$	15	F	F	F
5	$Pb_{0.80}M'_{0.20}F_{2.20}$	20	F	F	F + R
6	$Pb_{0.75}M'_{0.25}F_{2.25}$	25	F	F	F + R
7	$Pb_{0.70}M'_{0.30}F_{2.30}$	30	F	F + R	F + R
8	$Pb_{0.65}M'_{0.35}F_{2.35}$	35	F + H	F + R	F + R
9	$Pb_{0.60}M'_{0.40}F_{2.40}$	40	F + H	R	R
10	$Pb_{0.55}M'_{0.45}F_{2.55}$	45	F + H	R + O	T
11	$Pb_{0.50}M'_{0.50}F_{2.50}$	50	F + H	R + O	T
12	$Pb_{0.45}M'_{0.55}F_{2.55}$	55	F + H	R + O	T + O
13	$Pb_{0.40}M'_{0.60}F_{2.60}$	60	F + H	R + O	T + O
14	$Pb_{0.35}M'_{0.65}F_{2.65}$	65	F + H	R + O	T + O
15	$Pb_{0.30}M'_{0.70}F_{2.70}$	70	F + H	R + O	T + O
16	$Pb_{0.25}M'_{0.75}F_{2.75}$	75	F + H	R + O	T + O
17	$Pb_{0.20}M'_{0.80}F_{2.80}$	80	F + H	R + O	T + O
18	$Pb_{0.15}M'_{0.85}F_{2.85}$	85	F + H	R + O	T + O
19	$Pb_{0.10}M'_{0.90}F_{2.90}$	90	F + H	R + O	T + O
20	$Pb_{0.05}M'_{0.95}F_{2.95}$	95	F + H	R + O	T + O
21	$Pb_{0.00}M'_{1.00}F_{3.00}$	100	H	O	O

C = Cubic (fluorite) type, H = NdF_3 (hexagonal tysonite type), R = Rhombohedral, T = Tetragonal, O = ErF_3 or EuF_3 (orthorhombic YF_3 type).

splitting of reflections at $2\theta \sim 44°$, 52° suggests distortion in the fluorite lattice. The weak reflections become more prominent at the nominal composition $Pb_{0.60}Eu_{0.40}F_{2.40}$. A comparison of these XRD patterns to the similar compositions in BaF_2–ErF_3 or YF_3 [24,28,31], BaF_2NdF_3 [29,32] or PbF_2–YF_3 [16,21] systems suggests a rhombohedral ordering of the fluorite lattice in the present case also. All these systems contain rhombohedral phase with ideal composition $M_4^{2+}M'^{3+}_3F_{17}$ compositions. This phase was reported to exist in a narrow range of compositions, viz. 40–44 mol% of YF_3 [11]. The ideal composition of this rhombohedral phase should be $Pb_4Eu_3F_{17}$. A comparison of the XRD patterns of the nominal composition $Pb_{0.70}Eu_{0.30}F_{2.30}$, $Pb_{0.65}Eu_{0.35}F_{2.35}$ and $Pb_{0.60}Eu_{0.40}F_{2.40}$ shows that all the observed reflections in the former two compositions are broadened significantly. A careful observation of the peak shape of intense reflections shows that the broadened reflections are nothing but convolution of the peaks arising from two different phases. However, it needs to be mentioned here that any clear spilt reflections attributable to the rhombohedral phase could not be observed in the PbF_2–EuF_3 system. The unit cell parameters of $Pb_{0.60}Eu_{0.40}F_{2.40}$ were determined by analogy to the corresponding compositions, namely, $Ba_{0.60}Eu_{0.40}F_{2.40}$ and $Pb_{0.60}Er_{0.40}F_{2.40}$ like phases. The XRD pattern for nominal composition $Pb_{0.55}Eu_{0.45}F_{2.45}$ shows the presence of orthorhombic EuF_3. The XRD pattern of nominal composition $Pb_{0.60}Er_{0.40}F_{2.40}$ in PbF_2–ErF_3 system shows similar kind of weak reflections. This indicates that the ordered phases observed in both the systems are similar. The typical observed reflections for $Pb_{0.60}Eu_{0.40}F_{2.40}$ and $Pb_{0.60}Er_{0.40}F_{2.40}$, excluding the weak reflections, could be indexed on a rhombohedral lattice with unit cell parameters: $a = 4.132(1)$ and $c = 10.119(1)$ Å, and $a = 4.078(1)$ and $c = 10.006(3)$ Å, respectively. By the comparison of the XRD patterns of the present phases ($Pb_{0.60}Eu_{0.40}F_{2.40}$ and $Pb_{0.60}Er_{0.40}F_{2.40}$) with those of $Pb_4Y_3F_{17}$ [21] $Ba_4Eu_3F_{17}$ [31] and $Ba_4Y_3F_{17}$ [34], a larger rhombohedral unit cell and space group $R-3$ (No. 148) is proposed. This larger unit cell represents the superstructure of the former smaller (basis cell) unit cell. The typical basis and superstructure unit cell parameters are:

$Pb_{0.60}Eu_{0.40}F_{2.40}$

$a = 4.132(1)$, $c = 10.119(1)$ Å and $V = 149.62(3)$ Å^3 (basis structure);
$a = 10.928(3)$, $c = 20.278(11)$ Å and $V = 2097.0(1.3)$ Å^3 (superstructure).

$Pb_{0.60}Er_{0.40}F_{2.40}$

$a = 4.078(1)$, $c = 10.006(3)$ Å and $V = 144.12(7)$ Å^3 (basis structure);
$a = 10.804(2)$, $c = 19.962(6)$ Å and $V = 2017.9(9)$ Å^3 (superstructure).

The typical miller indices of the observed reflections for $Pb_{0.60}Eu_{0.40}F_{2.40}$ and $Pb_{0.60}Er_{0.40}F_{2.40}$, in both the

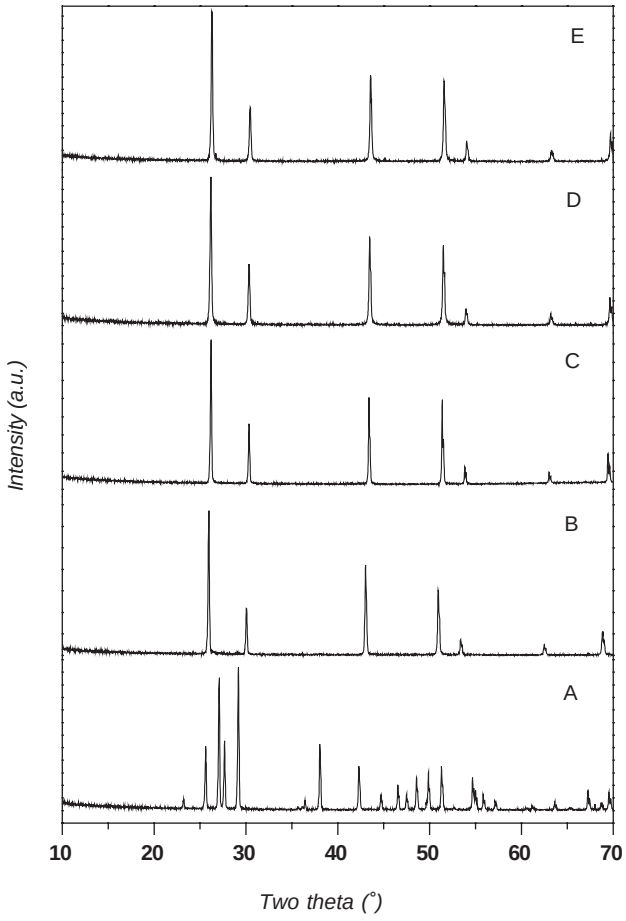

Fig. 1. Powder XRD patterns of PbF_2 and various solid solutions; A: α-PbF_2 (orthorhombic), B: β-PbF_2 (cubic), C: $Pb_{0.70}Nd_{0.30}F_{2.30}$, D: $Pb_{0.75}Eu_{0.25}F_{2.25}$ and E: $Pb_{0.85}Er_{0.15}F_{2.15}$.

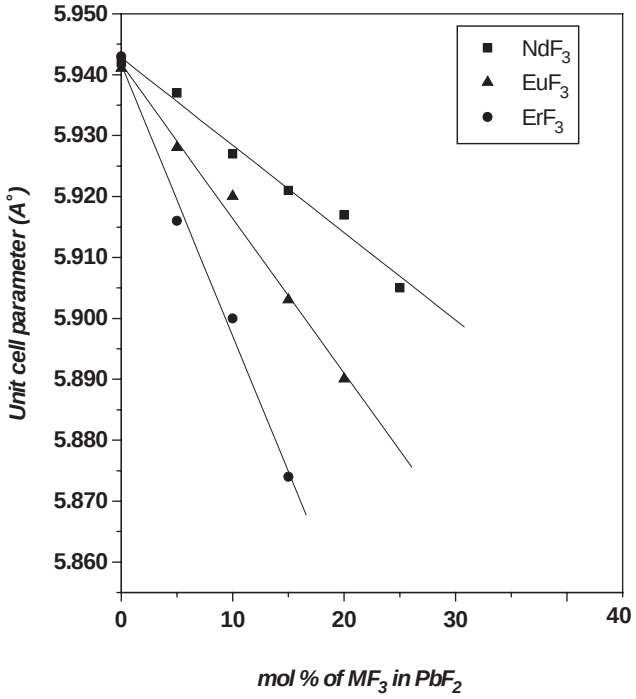

Fig. 2. Variation of unit cell volume as a function of $M'F_3$ content in the fluorite-type solid solution.

Table 5
Observed and calculated reflections for $Pb_{0.60}Eu_{0.40}F_{2.40}$

S. No.	$d_{(obs)}$ (Å)	I/I_0 (%)	$d_{(cal)}$ (Å) (1)	hkl (1)	hkl (2)	hkl (3)
1	3.738	3	3.728	1 0 5	2 2 1	
2	3.529	2	3.522	2 1 1	2 −1 0	
3	3.376	100	3.373	2 1 2	2 1 −1	1 0 1
4	2.922	45	2.923	2 1 4	3 1 0	1 0 2
5	2.602	1	2.603	3 1 1	2 −2 1	
6	2.540	2	2.541	3 1 2	3 −1 0	
7	2.470	1	2.471	2 0 7	3 3 1	
8	2.352	2	2.350	4 0 1	3 −1 −1	
9	2.251	3	2.251	2 1 7	4 2 1	
10	2.124	1	2.125	2 2 6	4 2 0	
11	2.066	64	2.065	4 1 0	3 −2 −1	1 0 4
12	2.043	2	2.044	4 0 5	3 3 −1	
13	1.762	54	1.762	4 1 6	4 3 −1	1 1 3
14	1.737	3	1.737	3 2 7	5 2 0	
15	1.686	2	1.687	4 2 4	4 2 −2	0 0 6
16	1.461	8	1.461	4 2 8	6 2 0	2 0 4

Typical unit cell parameters: (1). Hexagonal (supercell): $a = 10.928(3)$, $c = 20.278(11)$ Å and $V = 2097.0(1.3)$ Å^3; (2). Rhomb. (supercell): $a = 9.245(3)$ Å, $\alpha = 72.48(3)°$, and $V = 699.0(4)$ Å^3; (3). Hexagonal (basiscell): $a = 4.132(1)$, $c = 10.119(1)$ Å and $V = 149.62(3)$ Å^3. Corresponding rhombohedral cell: $a = 4.125(1)$, $\alpha = 60.17(1)$ and $V = 49.84(2)$ Å.

hexagonal and rhombohedral settings are summarized in Tables 5 and 6, respectively. The observed powder XRD patterns of these two nominal compositions are shown in Fig. 3. These basis and superstructure unit cells are, however, closely related among themselves and also to the parent fluorite lattice in an approximate relation as: $a_{super} = \sqrt{7} \times a_{sub}$ and $c_{super} = 2 \times c_{sub}$; $a_{sub} = \sqrt{2} \times a_f$ and $c_{sub} = \sqrt{3} \times a_f$ (the subscripts super and sub represent the superstructure and basis structure lattice parameters and the subscript f is used to indicate for parent fluorite unit cell). Such relations between rhombohedral and fluorite unit cells have been explained in several reports [19,33,34].

To characterize the exact nature of the rhombohedral phase, ideal stoichiometric composition $Pb_4Er_3F_{17}$ was prepared under similar experimental conditions. A detailed XRD analysis was carried out to elucidate the crystal structure of this phase. The powder XRD pattern shows a clear doublet like feature at $2\theta \sim 44°$ (corresponding to rhombohedral distortion of 220 reflection of parent fluorite lattice). Besides, this phase contains a number of weak reflections, at $2\theta \sim 21$, 24, 25, 34, 35, 36, 38, 40, etc. (can be seen from inset of Fig. 4), which indicate the superstructure formation in the rhombohedral lattice. The observed powder profile was refined by Rietveld method using the *Fullprof 2000* software package [35]. The initial position coordinates for various

Table 6
Observed and calculated reflections for $Pb_{0.60}Er_{0.40}F_{2.40}$

S. No.	$d_{(obs)}$ (Å)	I/I_0 (%)	$d_{(cal)}$ (Å) (1)	hkl (1)	hkl (2)	hkl (3)
1	4.206	<1	4.194	1 1 3	2 1 0	
2	3.671	1	3.672	1 0 5	2 2 1	
3	3.487	2	3.482	2 1 1	2 −1 0	
4	3.332	100	3.333	2 1 2	2 1 −1	1 0 1
5	2.886	45	2.885	2 1 4	3 1 0	1 0 2
6	2.503	2	2.503	2 2 3	3 1 −1	
7	2.323	<1	2.323	4 0 1	3 −1 −1	
8	2.217	3	2.218	0 0 9	3 3 3	
9	2.100	1	2.099	3 2 2	3 −2 1	
10	2.042	45	2.042	4 1 0	3 −2 −1	1 0 4
11	2.037	35	2.039	2 1 8	4 3 1	1 1 0
12	1.740	42	1.740	4 1 6	5 1 0	1 1 3
13	1.713	1	1.714	2 2 9	5 3 1	
14	1.693	1	1.692	2 0 11	5 3 3	
15	1.667	10	1.667	4 2 4	4 2 −2	0 0 6
16	1.533	<1	1.534	4 3 1	4 −3 0	
17	1.443	6	1.443	4 2 8	6 2 0	2 0 4

Typical unit cell parameters: (1). Hexagonal (supercell): $a = 10.804(2)$, $c = 19.962(6)$ Å and $V = 2017.9(9)$ Å^3; (2). Rhomb. (supercell): $a = 9.121(3)\mathring{A}$, $\alpha = 72.64(3)^\circ$, and $V = 672.7(3)$ Å^3; (3). Hexagonal (basis-cell): $a = 4.078(1)$, $c = 10.006(3)$ Å and $V = 144.12(7)$ Å^3. Corresponding rhombohedral cell: $a = 4.086(2)$, $\alpha = 59.87(2)$ and $V = 48.08(3)$ Å.

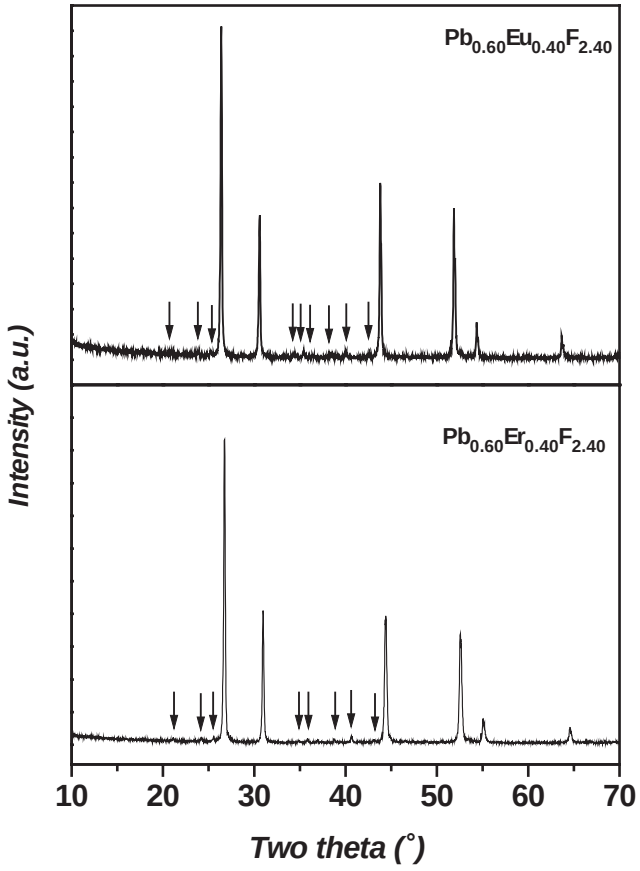

Fig. 3. Observed powder XRD pattern for nominal compositions $Pb_{0.60}Eu_{0.40}F_{2.40}$ and $Pb_{0.60}Er_{0.40}F_{2.40}$ (super-structure reflections are indicated by arrows).

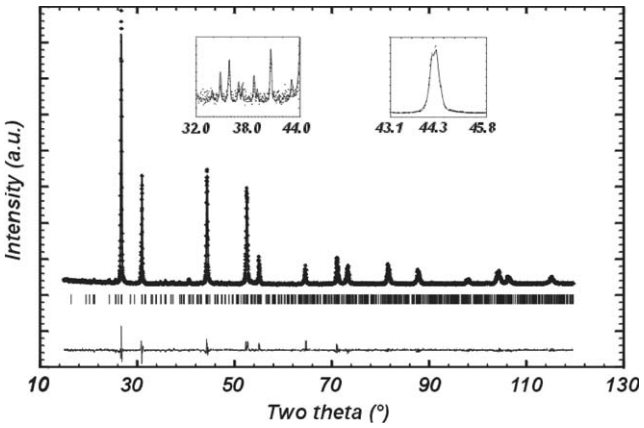

Fig. 4. Observed and calculated XRD patterns of $Pb_4Er_3F_{17}$. The difference plot is given below the pattern. The typical possible Bragg reflections are indicated by the vertical marks below the Rietveld plot.

Table 7
Typical crystallographic data and refined parameters for $Pb_4Er_3F_{17}$

Sample description	$Pb_4Er_3F_{17}$
Temperature	25°C
Crystal system and space group	Rhombohedral, R-3 (No. 148)
a and c (Å)	10.8190 (2) and 19.9513 (8)
V (Å^3) and Z	2022.4(1)
Profile parameters: (U, V, W)	0.075(7), −0.050(6), 0.033(2)
X and η	0.011(1) and 0.29(1)
Asymmetry parameters: A1 and A2	0.092(5), 0.044(2)
R_p, R_{wp} and R_{exp}	10.1%, 13.2% and 9.44%
χ^2	1.97
R_B	6.5%

atoms and space group are taken from the reported crystal structure of $Ba_4Y_3F_{17}$ [20]. The profile is fitted with pseudo-Voigt profile function. Initially scale and background are corrected with approximately accurate unit cell and profile parameters. The background is fitted with a fifth-order polynomial function. Further preferred orientation correction is applied using Rietveld function. The asymmetry correction is done with two-term asymmetry function. The refined unit cell parameters of $Pb_4Er_3F_{17}$ are: $a = 10.8190(2)$ and $c = 19.9513(8)$ Å, $V = 2022.44(1)$ Å^3. The details of other refined parameters and residuals of refinements are given in Tables 7 and 8. The typical Rietveld refinement plot showing the observed and calculated diffraction pattern along with the difference plot is shown in Fig. 4. The insets in the figure indicate some of the weak super structure reflections and typical split reflection. The vertical marks at the bottom indicate Bragg positions of a large number of possible refection.

The crystal structure analysis of this phase shows two crystallographically different lead atoms and one distinct erbium atom (in the ratio of 6:18:18) in the unit cell. There are eight different kinds of fluorine atoms in the unit cell. Erbium atoms are coordinated with the

Table 8
Position coordinates of various atoms of $Pb_4Er_3F_{17}$ in the unit cell

Atom	site	Occ.	x	y	z
Pb1	6*c*	1	0	0	0.2611(3)
Pb2	18*f*	1	0.2304(4)	0.0338(4)	0.0856(2)
Er1	18*f*	1	0.0866(4)	0.6128(3)	0.0785(2)
F1	18*f*	1	0.056(4)	0.786(3)	0.032(2)
F2	18*f*	1	0.430(4)	0.293(3)	0.112(2)
F3	18*f*	1	0.485(5)	0.096(3)	0.042(3)
F4	18*f*	1	0.207(3)	0.506(4)	0.039(1)
F5	18*f*	1	0.266(4)	0.383(2)	0.174(1)
F6	6*c*	1			0.134(4)
F7	3*a*	1	0	0	0
F8[a]	18*f*	0.167	0.948	0.930	0.494

$B_{overall} = 0.61(2)$ Å^2.
[a] Position coordinates of F8 atom is not included in the refinements. They are kept fixed at the given values.

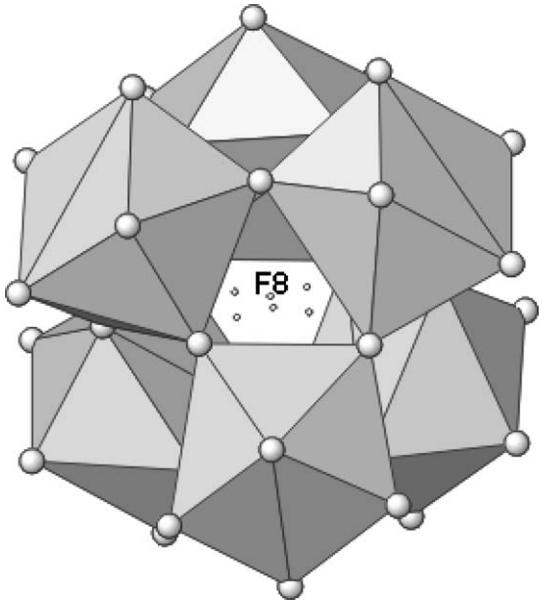

Fig. 5. A typical Er_6F_{36+1} cluster of $Pb_4Er_3F_{17}$, ErF_8 polyhedra are shown and the inner smaller spheres indicate the F8 atoms.

eight fluorine atoms forming a square anti-prism. Six of the ErF_8 square anti-prisms share the corners of one of their square face and form Er_6F_{36} cluster. The Er_6F_{36} cluster is the building block of many of the anion-excess fluorite related compounds. The Pb1 and Pb2 are 10 and 11 coordinated with the fluoride ions. The typical arrangements of all the atoms are similar to the reported structure of $Ba_4Y_3F_{17}$ [20] and $Ba_4Er_3F_{17}$ [31]. The typical Er–F bonds range from 2.26 to 2.40 Å. The Pb1–F bond lengths range from 2.50 to 2.72 Å. The Pb2 exists as a highly distorted 11-coordinated polyhedron with bonds ranging from 2.37 to 3.34 Å. A representative Er_6F_{36} cluster is shown in Fig. 5. The F4 and F5 atoms of the Er_6F_{36} cluster form a cubo-octahedron. One additional F8 fluorine atom is distributed over the 18*f* sites inside the cubo-octahedron cluster, and thus the Er_6F_{36} cluster can be better explained as Er_6F_{37} cluster. It needs to be mentioned here that the F8 atom position is not refined in the Rietveld refinement cycles. The powder XRD pattern of the corresponding phase $Pb_4Eu_3F_{17}$ is closely similar to the $Pb_4Er_3F_{17}$. The detailed XRD study of this phase is in progress and will be communicated separately.

In the PbF_2NdF_3 system, beyond the solid solution limit, i.e., compositions subsequent to $Pb_{0.70}Nd_{0.30}F_{2.30}$ show reflections attributable to NdF_3. This indicates that there are no other phases present in this system except the fluorite-type solid solution and NdF_3 phases. Similarly, in PbF_2–EuF_3 system, compositions beyond the rhombohedral phase, i.e., $Pb_{0.55}Eu_{0.45}F_{2.55}$ and so on, show the presence of EuF_3 reflections. From this observation, it can be inferred that no other phases, except the fluorite-type solid solution and rhombohedral phase, are observed in this system.

The XRD pattern of the nominal composition $Pb_{0.55}Er_{0.45}F_{2.45}$, which follows the rhombohedral ordered phase in PbF_2–ErF_3 system, shows the absence of all the weak reflections present in the nominal composition $Pb_{0.60}Er_{0.40}F_{2.40}$. The typical fluorite peak positions at $2\theta \sim 31°$ and 52° appear as doublets in the XRD pattern. In addition, the presence of weak reflections at $2\theta \sim 34°$ and 37° are additional features in the XRD pattern of this composition. A typical XRD pattern of $Pb_{0.55}Er_{0.45}F_{2.45}$ is shown in Fig. 6. Thus, it was considered as a new phase different from the above explained fluorite related rhombohedral phase. This phase is quite similar to tetragonal [11] and orthorhombically distorted tetragonal [16] phases observed in PbF_2–YF_3 system. A similar XRD pattern was also observed at the nominal composition $Pb_{0.50}Er_{0.50}F_{2.50}$. Beyond this nominal composition, the other compositions were found to contain reflections due to ErF_3. The observed reflections for the $Pb_{0.55}Er_{0.45}F_{2.45}$ and

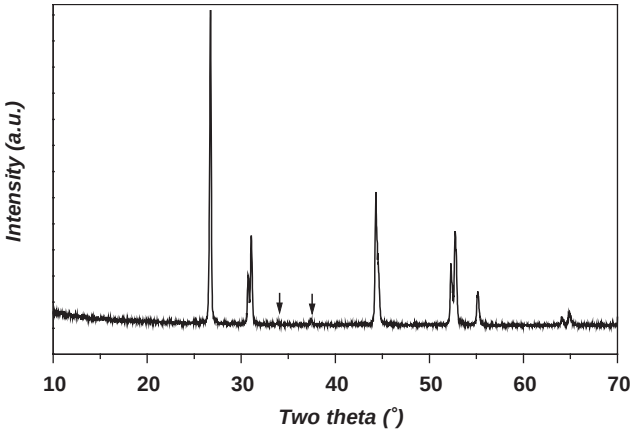

Fig. 6. Observed powder XRD pattern for nominal composition $Pb_{0.55}Er_{0.45}F_{2.45}$ (super-structure reflections are indicated by arrows).

Table 9
Observed and calculated reflections for $Pb_{0.55}Er_{0.45}F_{2.45}$

S. No.	$d_{(obs)}$ (Å)	I/I_0 (%)	$d_{(cal)}$ (Å) (1)	hkl (1)	$d_{(cal)}$ (Å) (2)	hkl (2)
1	3.953	<1			3.958	101
2	3.334	100	3.331	101	3.331	103
3	2.909	17	2.906	002	2.907	006
4	2.878	29	2.874	110	2.874	110
5	2.649	<1			2.647	105
6	2.401	1			2.400	114
7	2.044	47	2.043	112	2.044	116
8	2.032	19	2.032	200	2.032	200
9	1.748	23	1.749	103	1.749	109
10	1.735	34	1.735	211	1.735	213
11	1.665	12	1.665	202	1.666	206
12	1.454	4	1.453	004	1.454	0012
13	1.436	4	1.437	220	1.437	220

Typical unit cell parameters: (1) $a = 4.064(1)$, $c = 5.811(2)$ Å and $V = 96.00(4)$ Å^3; (2) $a = 4.064(1)$, $c = 17.442(4)$ Å and $V = 288.1(1)$ Å^3.

$Pb_{0.50}Er_{0.50}F_{2.50}$ excluding the weak reflections could be indexed on a tetragonal lattice (basis lattice). To include the weak reflections, the c-axis of the tetragonal unit cell had to be tripled. A list of the observed and calculated reflections for the nominal composition $Pb_{0.55}Er_{0.45}F_{2.45}$ is given in Table 9. The typical unit cell parameters of the tetragonal phases observed in the compositions $Pb_{0.55}Er_{0.45}F_{2.45}$ and $Pb_{0.50}Er_{0.50}F_{2.50}$ are:

$Pb_{0.55}Er_{0.45}F_{2.45}$

$a = 4.064(1)$, $c = 5.811(2)$ Å and $V = 96.00(4)$ Å^3 (basis lattice);
$a = 4.064(1)$, $c = 17.442(4)$ Å and $V = 288.1(1)$ Å^3 (superstructure lattice).

$Pb_{0.50}Er_{0.50}F_{2.50}$

$a = 4.046(1)$, $c = 5.796(2)$ Å and $V = 94.86(5)$ Å^3 (basis lattice);
$a = 4.046(1)$, $c = 17.386(6)$ Å and $V = 284.5(1)$ Å^3 (superstructure lattice).

These unit cell parameters bear close relation to the parent fluorite unit cell. The typical relation between the unit cell parameters of the tetragonal unit cell and the parent fluorite unit cell are as: $a_{t(basis)} \approx a_f/\sqrt{2}$ and $c_{t(basis)} \approx a_f$ and the exact cell parameters are: $a_t = a_{t(basis)}$ and $c_t = 3 \times c_{t(basis)}$, where the subscript 't' and 'f' indicate the tetragonal and fluorite unit cells, respectively. Reau et al. [11] have reported a similar composition close to $PbYF_5$ (i.e., at about 49 mol% of YF_3) with a tetragonal unit cell having 4.076(2) and 17.400(5) Å, as a and c parameters, respectively. Earlier closely related tetragonal unit cells have been proposed for Pb_2YF_7 ($a_t = 4.080(1)$ and $c_t = 17.392(4)$ Å) [12] and Ca_2YbF_7 ($\sim 2 \times a_t$ and c_t) type compositions [36] (tetragonal unit cell parameters for Ca_2YbF_7 are reported as: 8.673(0) and 16.577(1) Å).

The indices of the observed powder XRD pattern of $Pb_{0.55}Er_{0.45}F_{2.45}$ (Table 9) suggests $I4/mmm$ space group for this phase. Earlier Dib et al. [12] have reported similar unit cell parameters for Pb_2YF_7 composition, but they assigned space group $I4$ or $I4/m$. Ness et al. [36] have proposed $2 \times a_t$ and c_t as unit cell parameter for a closely similar composition Ca_2YbF_7 in CaF_2–YbF_3 system. They assigned space group $I4/m$ for this structure. In this structure they have reported a randomization of several Ca and Yb atoms in the lattice. In their structural report they have proposed partial occupancy of Ca^{2+}, Yb^{3+} in 8h, 4e and 2b sites, with square anti-prism or cubical coordination polyhedra. The Ca^{2+} in 16i sites have a 10-coordinated polyhedron. A similar arrangement with 8h, 4e and 2b site with Er^{3+} and 16i for Pb^{2+} is expected for the present composition. The present powder XRD data, however, do not show any indication for space group $I4/m$, hence, we could not use this model for our study. The exact structural arrangement of this phase will be carried out and will be reported subsequently.

A careful analysis of the XRD pattern of $Pb_{0.50}Er_{0.50}F_{2.50}$ indicates the presence of a very small amount of ErF_3. The intensity of the reflections attributable to ErF_3 increases in the subsequent compositions. This suggests that the tetragonal phase exists with slightly less than 50 mol% as observed by Reau et al. for PbF_2–YF_3 [11] system. All other following compositions yield a mixture of the tetragonal phase of the type $Pb_{0.55}Er_{0.45}F_{2.45}$ and the leftover ErF_3.

It was also revealed that no PbF_2 could be retained in any of the three rare-earth fluoride lattices. This was further verified from the determination of unit cell parameters of the rare-earth fluoride phases in the different nominal compositions. Earlier it was reported in BaF_2–$M'F_3$ (where $M' = Y^{3+}$, Er^{3+}, Eu^{3+}) systems that no BaF_2 can be incorporated into YF_3, ErF_3 and EuF_3 lattices [24,28]. The presently studied PbF_2–EuF_3 and PbF_2–ErF_3 systems also show similar results. But in the case of MF_2–NdF_3 ($M = Ba^{2+}$, Sr^{2+} and Ca^{2+}) systems, about 10-mol% of MF_2 could be retained in the NdF_3 lattice [29,30]. However, no PbF_2 could be incorporated into the NdF_3 lattice. Besides, no tysonite-type phase or Er_2BaF_8 type phase was observed in these studied systems.

The summary of the phase relations in the three studied systems is shown as bar diagram in Fig. 7. In each segment, the extreme left end indicates the fluorite-type solid solution and the extreme right end indicates the rare-earth fluoride lattice. A comparison of the three studied systems reveals that the fluorite-type solid solution is the only common feature in them. The rhombohedral ordered phase were observed both in the PbF_2–EuF_3 and PbF_2–ErF_3 systems, but not in the

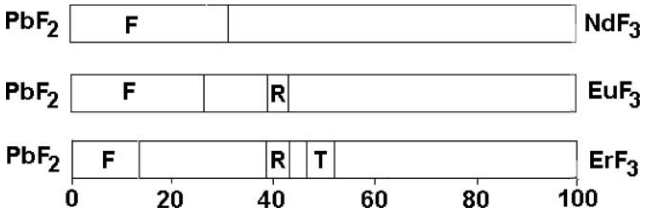

Fig. 7. Summary of phase relations in $Pb_{1-x}M'_xF_{2+x}$ systems (bar representation) F = Fluorite, R = Rhombohedral, T = Tetragonal Unmarked zones (biphasic) contain two neighboring phases.

PbF_2–NdF_3 system. The tetragonal ordered phase is observed only in PbF_2–ErF_3 system.

In the earlier phase relation studies in MF_2–$M'F_3$ systems, it was observed that the typical solid solution limit increases with the decrease in the difference in the ionic radii of the M^{2+} and M'^{3+} cations [27,30]. A similar conclusion was also drawn in the present studied systems, i.e., the typical solid solution limit increases from PbF_2–ErF_3 to PbF_2NdF_3 system, viz. 15–30 mol% with change in rare-earth ion from Er^{3+} to Nd^{3+}. The formation of the rhombohedral phase in PbF_2–EuF_3, PbF_2–ErF_3 or PbF_2–YF_3 systems indicates that the ionic radii of M^{2+} and M'^{3+} plays a significant role in the formation of the rhombohedral ordered phase. Such rhombohedral phase was observed with NdF_3 only when the counter cation is Ba^{2+}. From, these observations it can be suggested that the rhombohedral and other ordered phases are possible, only when there is a significant difference in the ionic radii of M^{2+} and M'^{3+}. The formation of the tetragonal phase only in PbF_2–ErF_3 and PbF_2–YF_3 [16] systems (within 45–50 mol% of $M'F_3$), suggests the ionic radii of the rare-earth ion has an important role in its stabilization. However, the rhombohedral phase is observed in wide range of rare-earth ions. Fedorov et al. had reported the PbF_2–$M'F_3$ ($M' = Ho^{3+}$, Yb^{3+} and Sc^{3+}) phase equilibria from the phase analysis of the quenched samples [15]. In all these phase equilibria they had not observed any tetragonal phase neither at 33 or 50-mol% of $M'F_3$. A comparison of the results obtained in the present study with those of Reau et al. [11], Dib et al. [12] and Fedorov et al. [15] suggests the preparation conditions, namely, heating temperature, annealing time and cooling protocol also play equally important role in governing the phase equilibria. Except the study made by Reau et al., all other literature studies [11,15] are based on the long annealed samples. Thus, at present it is concluded that besides the optimally different ionic radii of the guest and host ions, the short annealing conditions are ideal for the formation of such a tetragonal phase.

In any of these three systems, PbF_2 did not show any solubility in the $M'F_3$ lattices. However, in the earlier studies on MF_2–NdF_3 ($M = Ca^{2+}$, Sr^{2+} and Ba^{2+}) systems solubility of M^{2+} in NdF_3 was reported [29,30]. This may be because of higher electropositive character of the alkaline-earth metals than lead. Thus, the solubility of M^{2+} in $M'F_3$ lattice is not only governed by the radius of the metal ions but also by the nature of the metal ion.

The PbF_2–$M'F_3$ systems, more closely resemble with the BaF_2–$M'F_3$ system, despite the fact that ionic radius of Pb^{2+} is very close to that of Sr^{2+}. However, many differences between PbF_2–$M'F_3$ and BaF_2–$M'F_3$ systems are also observed, which are due to a considerable difference between ionic radii and electro-positive character difference between the alkaline earth metal ions and Pb^{2+}. Thus, the ionic radii of the M'^3 cation has a governing role in the formation of the ordered phases or deciding width of solid solution in MF_2–$M'F_3$ phase equilibria. Smaller difference between the ionic radii facilitates the solid solution formation whereas the larger difference leads to the cations segregation which results in ordered structure formation.

4. Conclusions

From the foregoing, the phase relations in PbF_2–$M'F_3$ ($M' = Nd^{3+}$, Eu^{3+} and Er^{3+}) under short annealed and slow cooled conditions are established. The typical solid solution limit of NdF_2, EuF_3 and ErF_3 in PbF_2 are 30, 25 and 15-mol%, respectively. A rhombohedral fluorite related ordered phased was observed in PbF_2–EuF_3 and PbF_2–ErF_3 systems near the composition $Pb_{0.60}M_{0.40}F_{2.40}$. A tetragonal fluorite related ordered phase is observed only in PbF_2–ErF_3 system. No tysonite or tysonite related phases are observed in these systems. In addition, no solubility of the PbF_2 in the rare-earth fluorides is observed in the present study.

Acknowledgments

The authors thank Dr. N.M. Gupta, Head Applied Chemistry Division for his keen interest in this work.

References

[1] K. Koto, H. Schultz, R.A. Huggins, Solid State Ionics 1 (1980) 355.
[2] J.M. Reau, P. Hagenmuller, Appl. Phys. A 49 (1989) 3.
[3] M.W. Shafer, G.V. Chandrasekhar, R.A. Figat, Solid State Ionics 5 (1981) 633.
[4] J.P. Laval, A. Mikou, B. Frit, G. Roult, Solid State Ionics 28–30 (1988) 1300.
[5] J.M. Reau, M. Wahbi, J. Senegas, P. Hagenmuller, Phys. Stat. Sol. (b) 169 (1992) 331.
[6] S.J. Patwe, P. Balya, P.S. Goyal, A.K. Tyagi, Mater. Res. Bull. 36 (2001) 1743.
[7] D.C. Stockbarger, J. Opt. Soc. Am. 39 (1970) 731.

[8] P.A. Tick, N.F. Borreli, I.M. Reaney, Opt. Mater. 15 (2000) 81.
[9] M. Mortier, P. Goldner, C. Chatteau, M. Genotelle, J. Alloys Compounds 323–324 (2001) 245.
[10] M.A.P. Silva, V. Briois, M. Poulain, Y. Messaddeq, S.J.L. Ribeiro, J. Phys. Chem. Solids 64 (2003) 95.
[11] J.M. Reau, P.P. Fedorov, L. Rabardel, S.F. Matar, P. Hagenmuller, Mater. Res. Bull. 18 (1983) 1235.
[12] A. Dib, S. Aleonard, M.T. Roux, J. Solid State Chem. 52 (1984) 292.
[13] P.P. Fedorov, I.P. Zibrov, B.P. Sobolov, I.V. Shishkin, Russ. J. Inorg. Chem. 32 (1987) 1794.
[14] P.P. Fedorov, I.P. Zibrov, E.V. Tarasova, S.M. Polunina, P.I. Fedorov, B.P. Sobolev, Russ. J. Inorg. Chem. 33 (1988) 1863.
[15] P.P. Fedorov, V. Trnovcova, V.A. Melashina, V.D. Chugunov, B.P. Sobolov, Inorg. Mater. 30 (1994) 384.
[16] S.J. Patwe, S.N. Achary, A.K. Tyagi, Mater. Res. Bull. 36 (2001) 597.
[17] A. Zalkin, D.H. Templeton, J. Am. Chem. Soc. 75 (1953) 2453.
[18] J.H. Kenedy, R. Miles, J. Hunter, J. Electrochem. Soc. 120 (1973) 1441.
[19] M. Kieser, O. Greis, Z. Anorg. Allg. Chim. 469 (1980) 164.
[20] B.A. Maksimov, Kh. Solans, A.P. Dudka, E.A. Genkina, M.F. Badria, I.I. Buchinskaya, A.A. Loshmanov, A.M. Golubev, V.I. Simonov, M.F. Altaba, B.P. Sobolev, Cryst. Rep. 41 (1996) 50.
[21] J. Köhler, S.N. Achary, A.K. Tyagi, Z. Kristallogr. 217 (2002) 23.
[22] O. Greis, J.M. Haschke, Rare earth fluorides, in: K.A. Gschneidner, L. Eyring (Eds.), Handbook on Physics and Chemistry of Rare earths, North-Holland, Holland, 1982 (Chapter 48).
[23] A.K. Cheetham, B.E.F. Fender, M.J. Cooper, J. Phys. C: Solid State Phys. 4 (1971) 3107.
[24] S.N. Achary, S.J. Patwe, A.K. Tyagi, Mater. Res. Bull. 37 (2002) 2227.
[25] N.B. Grigoreva, B.A. Maksimov, L.P. Otroshchenko, B.P. Sobolev, V.I. Simonov, Crystallgr. Rep. 43 (1998) 553.
[26] J.M. Reau, P. Haegenmuller, Rev. Inorg. Chem. 19 (1999) 45.
[27] S.N. Achary, S.J. Patwe, A.K. Tyagi, Mater. Res. Bull. 34 (1999) 2093.
[28] S.J. Patwe, S.N. Achary, A.K. Tyagi, Mater. Res. Bull. 37 (2002) 2243.
[29] V. Grover, S.N. Achary, S.J. Patwe, A.K. Tyagi, Mater. Res. Bull. 38 (2003) 1101.
[30] V. Grover, S.N. Achary, S.J. Patwe, A.K. Tyagi, Mater. Res. Bull. 38 (2003) 1413.
[31] A.K. Tyagi, J. Köhler, Solid State Sci. 3 (2001) 689.
[32] V. Grover, S.N. Achary, S.J. Patwe, A.K. Tyagi, Powder Diff. 17 (2002) 326.
[33] S.N. Achary, S.J. Patwe, A.K. Tyagi, Powd. Diff. 17 (2002) 225.
[34] E.F. Bertaut, Y. Le Fur, S. Aleonard, Z. Kristallogr. 187 (1989) 279.
[35] J. Rodriguez-Caravajal, Sattelite Mmeeting on Powder Diffraction, 15th Conference of the International Union of Cryst., Toulouse, France 127, 1990.
[36] S.E. Ness, D.J.M. Beven, H.J. Rossell, Eur. J. Solid State Inorg. Chem. 25 (1988) 509.